Astronomical and Astrophysical Transactions (*AApTr*), 2021, Vol. 32, Issue 2, pp. 131–136,
ISSN 1055-6796, Photocopying permitted by license only, ©Cambridge Scientific Publishers

Numerical simulation of three-dimensional collisionless disk of NGC 1566 galaxy

R.V. Zolotarev*, V.I. Korchagin, B.B. Jmailov, R.R. Dibirov

Institute of Physics, Southern Federal University, Stachki Ave., 194, Rostov-on-Don, 344090, Russia

Received 1 March, 2020

This paper reports the results of the numerical N-body simulations of the dynamics of collisionless disk of the galaxy NGC 1566. Using recent observational data for this galaxy, we construct equilibrium three-dimensional collisionless model of its disk, and study the disk dynamics using direct N-body simulations. Results of our simulations show that the most unstable global mode in the collisionless disk is the two-armed spiral. Estimate of the pattern speed of the two-armed spiral, emerging in the numerical simulations gives the value of 21.6 ± 1 km/s/kpc which is consistent with the pattern speed of the spiral $\Omega_p = 23 \pm 2$ km/s/kpc estimated from observations.

Keywords: Numerical simulations, GPGPU, NGC 1566

1 Introduction

The theory of spiral structure of galaxies remains in many aspects unresolved issue. Nearby isolated grand design galaxy NGC 1566 with its two-armed spiral pattern provides a good opportunity to test theoretical approaches in explaining the spiral structure in galaxies. Theoretical modeling of NGC 1566 was undertaken in the past by Korchagin et al. (2000) who used hydrodynamical approximation to model the dynamics of spiral structure in it. Korchagin et al. (2000) used available observational data and demonstrated that the hydrodynamical approximation explains well the number and the pitch angle of spiral arms in this galaxy.

Since then, the galaxy has been a subject of extensive photometric and spectroscopic studies. Recently a precisely measured gaseous rotation curve of the galaxy NGC 1566 has been obtained (Elagali et al. 2019), which was used to construct equilibrium model of its three-dimensional collisionless disk.

The modeling of spiral structure in NGC 1566 by Korchagin et al. (2000) was done using two-dimensional hydrodynamical approximation. The disks of spiral galaxies consist mostly of the collisionless stars. Numerical modeling of the collisionless gravitating disks is usually focused on the late stages of gravitational instability which,

*Email: rv_zolotarev@mail.ru

as a rule, is characterized by the development of a prominent bar. In modeling the spiral structure of the particular galaxies of interest is the linear stage of instability with exponential growth of perturbations and the early stages of the nonlinear stabilization of perturbations. At the linear stage of instability, the dynamics of the global modes is similar independently of whether the gravitating disk is described in the hydrodynamical, collisionless, or the collisionless-hydrodynamical approximations (Khoperskov et al. 2012). At the nonlinear stage of instability, the dynamics of gravitating disk depends on its nature. The collisionless gravitating disks demonstrate the development of a prominent bar, while gravitating gaseous disks break down onto two or more gravitating clumps. With presence of a gaseous component in the collisionless gravitating disks, the life time of the spiral pattern, developing during the linear stages of instability, increases up to a few Gyr (Khoperskov et al. 2012). Thus, the spiral structure, developing in the collisionless models at the linear stage of instability determines the morphology of the long-lived spiral structure in the collisionless–gaseous models.

In this paper we report the results of the modeling the dynamics of the three-dimensional collisionless disk with the rotation curve, velocity dispersion profiles, and the density distribution taken from observations of the disk of NGC 1566. Section 2 describes the equilibrium model of the galaxy and the numerical technique we use to model the dynamics of the galactic disk. Section 3 provides the results of our simulations, and gives a comparison of our theoretical modeling with observational data. Section 4 summarizes the results.

2 Equilibrium model and numerical technique

In modeling disk we use N-body approach taking account for the external gravity of the spherical component. At the first step we construct an equilibrium model of the disk with given spatial and velocity distribution. At the second step the model is calculated with direct N-body code. Mathematically, the problem consists of solving $6N$ differential equations of 1st order and setting initial conditions for them. The external potential is presented in two components: bulge (Plummer model) and DM halo (modified isothermal sphere) with following mass density distributions

$$\rho_b(r) = \rho_{b0}\left(1+\frac{r^2}{a_b^2}\right)^{-\frac{5}{2}}, \quad \rho_h(r) = \rho_{h0}\left(1+\frac{r^2}{a_h^2}\right)^{-1}. \tag{1}$$

Parameters of the distributions was obtained from rotation curve decomposition, $\rho_{b0} = 0.39\,\mathrm{M}_\odot\mathrm{kpc}^{-3}$, $a_b = 2.3\,\mathrm{kpc}$, $\rho_{h0} = 0.07\,\mathrm{M}_\odot\mathrm{kpc}^{-3}$, $a_h = 1.8\,\mathrm{kpc}$.

2.1 The equilibrium model

We use initial spatial distribution in the exponential form to be consistent with observational surface density profile $\Sigma \sim e^{-r/h}$ (Elagali et al. 2019)

$$\rho(r,z) = \frac{M_d}{4\pi h^2 z_0}\exp\left(-\frac{r}{h}\right)\mathrm{sech}^2\left(\frac{z}{z_0}\right), \tag{2}$$

where $M_d = 5.5 \cdot 10^{10}\,\mathrm{M}_\odot$ is total mass of the disk in model, $h = 4.2\,\mathrm{kpc}$ and $z_0 = 0.6\,\mathrm{kpc}$ is radial and vertical scale respectively. We use the isothermal sheet approximation to construct the disk equilibrium in the vertical direction. Visualization of the initial state is represented in Fig. 1 (left panel) and in Fig. 2 (dashed line). Observational data (Elagali et al. 2019) provide information about the gaseous rotation curve V_c which is a tracer of gravitational potential and can be used to obtain mass distribution. We use this data to construct rotation curve for model $\mathrm{v}(r)$. The velocity distribution of the model was constructed using Hernquist (1993) technique which is based on Jeans equations and assumes an absence of the systematic radial motions, the axial symmetry, the and its symmetry relative to the disk's mid-plane. Following Hernquist (1993), we take the initial rotation curve of the collisionless model $\mathrm{v}(r)$ and the velocity dispersion components c_r, c_θ, c_z as follows:

$$\mathrm{v}^2(r) = V_c^2(r) - c_\theta^2 + c_r^2\left(1 - 2\frac{r}{h}\right) \tag{3}$$

$$\begin{gathered} c_r^2 = c_0 \cdot \exp\left(-\sqrt{r^2 + 2a_s^2}/h\right) \\ c_\theta^2 = c_r^2 \frac{\varkappa^2}{4\Omega^2} \\ c_z^2 = \pi G \Sigma(r) z_0, \end{gathered} \tag{4}$$

where $V_c(r) = \sqrt{r\frac{\partial \Phi_{\mathrm{tot}}}{\partial r}}$, Φ_{tot} is total gravitational potential, determined by all components, $\Omega = \mathrm{v}(r)/r$, $a_s = 0.25h$ (Hernquist 1993, Quinn et al. 1993), $c_0 = 121\ \mathrm{km\,s^{-1}}$. The initial equilibrium rotation curve is shown in Fig. 3 (dashed line). Density distribution, velocity dispersion and rotation curve determine Toomre's Q-parameter (Toomre 1964)

$$Q = \frac{c_r \varkappa}{3.36 G \Sigma}, \tag{5}$$

which is an important measure of the stability of gravitating disk. In the constructed model, the value of Toomre's Q-parameter is greater than unity in all disk regions (Fig. 4).

2.2 Basic equations and numerical approach

The behavior of N-body system is described by equations of motion

$$\begin{cases} \dot{\vec{x}}_i = \vec{\mathrm{v}}_i \\ \dot{\vec{\mathrm{v}}}_i = \sum\limits_{\substack{j=1 \\ j \neq i}}^{N} \dfrac{m_j\,(\vec{x}_j - \vec{x}_i)}{r_{ij}^3} - \vec{\nabla}\Phi_{\mathrm{ext}}, i = 1, \ldots, N. \end{cases} \tag{6}$$

where $\vec{x}_j$, $\vec{\mathrm{v}}_j$, m_j is a coordinate, velocity and mass of a particle with number j, r_{ij} is the distance between the particles with numbers i and j, Φ_{ext} is gravitational potential of the external spherical component. The system is integrated with direct second-order symplectic leapfrog-KDK scheme with fixed timestep (Binney and Tremaine 2008). To avoid numerical divergence due to close encounters and the nonphysical binary formation, we use regularization in form of the Plummer model with softening length of $\delta = 40$ pc (Athanassoula et al. 2000). Experiments with variation of the

softening length do not affect significantly on the model behavior. All calculations were done with the parallel algorithm using GPU and CUDA. The key feature of the algorithm is usage of full-GPU cycle without an active use of host-RAM, which allows us to speed up the calculations.

3 Simulation results

Model was integrated up to 3 Gyr with $N = 286720$ particles and timestep $\Delta t = 0.05$ Myr. During simulation a number of spiral modes are formed. The two-armed mode is the most prominent one at the linear stage of instability. Snapshot of our simulation taken at time 1.5 Gyr is presented at Fig. 1. Our estimate of the pattern angular velocity for $m = 2$ mode is 21.6 ± 1 km/s/kpc which is in agreement with value of 23 ± 2 km/s/kpc measured for this galaxy by Agüero et al. (2004). Since the model is purely collisionless, the spiral structure does not live during all period of simulation and evolves into the elongated bar-like structure. The spirals persist during approximately of 0.5–0.7 Gyr.

The formation of the global structure does not sufficiently change the background density and the velocity distributions during the simulation time (see Fig. 2 and Fig. 3) with the average values of the surface density and the velocity distributions remaining close to the initial ones.

To analyze the structure formation, we use the Fourier series approach. To do that, the spatial distribution of the particles $\{\vec{x}_i\}_{i=1,\ldots,N}$ was converted to the surface mass density $\Sigma(r, \theta)$. At the next step, the Fourier transform is applied to surface density distribution. The amplitudes of the Fourier harmonics show the "intensity" of each global mode with the amplitude of m-th harmonic defined as

$$A_m = \frac{1}{M_d} \left| \int_0^{Rmax} r\, dr \int_0^{2\pi} d\theta \Sigma(r, \theta) e^{-im\theta} \right|. \tag{7}$$

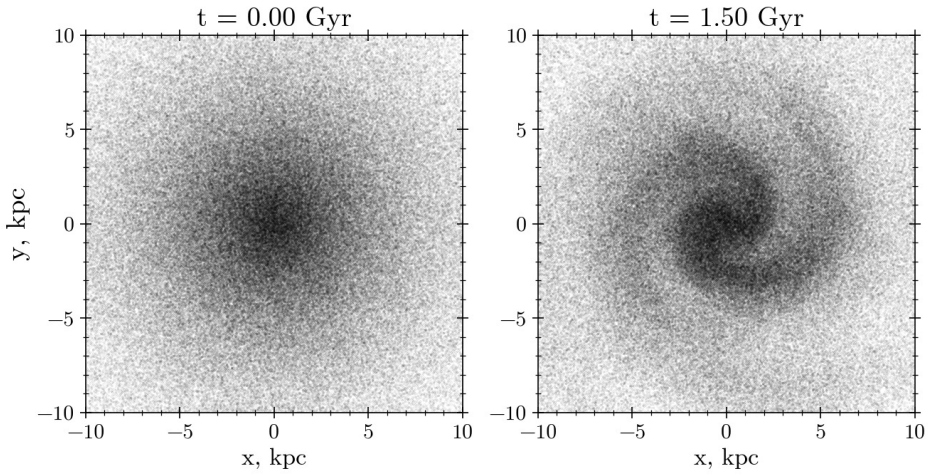


Figure 1 Model snapshots: initial (left), after 1.5 Gyr (right).

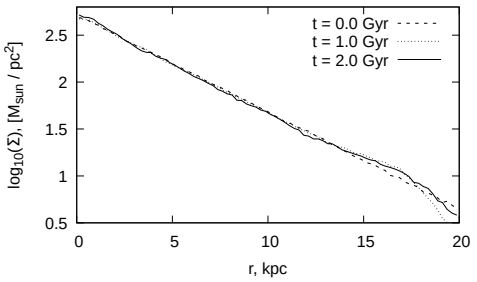


Figure 2 Surface density.

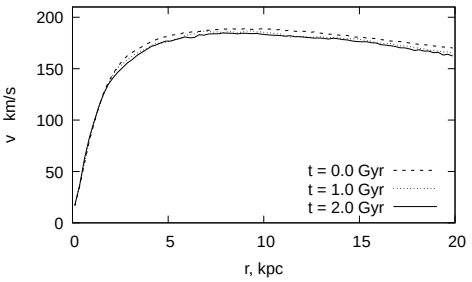


Figure 3 Rotation curve.

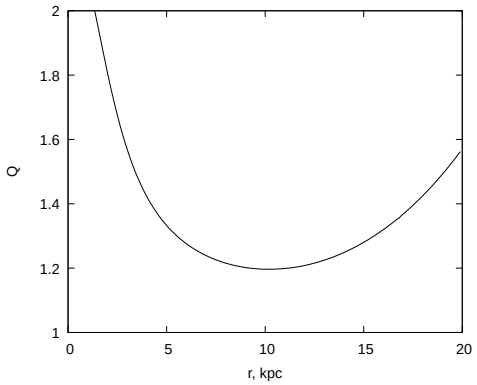


Figure 4 Q-parameter.

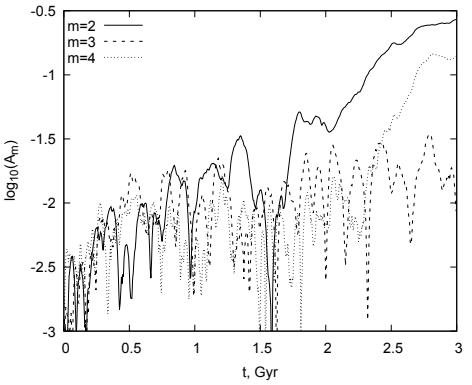


Figure 5 Evolution of global Fourier amplitudes.

Figure 5 plots a time dependence of the global Fourier amplitudes on time. The exponentially growing mode $m = 2$ dominates from 1.5 Gyr until the nonlinear saturation which starts starts at approximately 2.5 Gyr. Mode $m = 4$ also grows exponentially as well but saturates at a low level. The amplitude of two-armed mode reaches the value of $\log_{10}(A_2) = -0.5$ while the amplitude of $m = 3$ mode remains lower than –1.5.

4 Summary

This paper has focused on the study of the spiral structure in the collisionless disk of the galaxy NGC 1566. Using observational data, we constructed the equilibrium model of the disk of NGC 1566. To integrate disk dynamics, we used the direct N-body simulations. Our simulations demonstrate that the collisionless disk with the parameters close to those of NGC 1566 is unstable with respect to the growth of the global spiral modes. The mode $m = 2$ has the largest increment of instability. At the non-linear stage, the structure evolves into the bar-like structure due to collisionless nature of the model. The angular velocity of the spiral pattern estimated for

the two-armed spiral has the value 21.6 ± 1 km/s/kpc which in agreement with the observational value 23 ± 2 km/s/kpc (Agüero et al. 2004).

Acknowledgments

R.Z. and V.K. acknowledge financial support by Southern Federal University, 2020 (Ministry of Science and Higher Education of the Russian Federation). The authors thank an anonymous referee for valuable comments.

References

Agüero E. L., Díaz R. J., Bajaja E. (2004), A&A, 414, 453
Athanassoula E., Fady E., Lambert J. C., Bosma A. (2000), MNRAS, 314, 475
Binney J., Tremaine S. (2008), Galactic Dynamics: Second Edition
Elagali A., Staveley-Smith L., Rhee J. et al. (2019), MNRAS, 487, 2797
Hernquist L. (1993), ApJS, 86, 389
Khoperskov, S. A., Khoperskov, A. V., Khrykin, I. S., et al. (2012), MNRAS, 427, 1983
Korchagin V., Kikuchi N., Miyama S. M. et al. (2000), ApJ, 541, 565
Quinn P. J., Hernquist L., Fullagar D. P. (1993), ApJ, 403, 74
Toomre A. (1964), ApJ, 139, 1217